Ionospheric *D* region: VLF-measured Electron Densities compared with Rocket-Based FIRI-2018 Model

Neil R. Thomson[1], Mark A. Clilverd[2], and Craig J. Rodger[1]

[1]Physics Department, University of Otago, Dunedin, New Zealand

[2]British Antarctic Survey (UKRI-NERC), Cambridge, UK

Key Points:

- VLF-measured *D* region electron number densities are compared with the rocket-based FIRI-2018 model over heights 60-90 km
- Average VLF-measured nighttime electron number densities agree very well with the rocket-based FIRI-2018 model (at heights 75-90 km)
- By day there is reasonable agreement at low latitudes (at ~60-75 km), but at high mid-latitudes FIRI lacks galactic cosmic ray effects

Abstract

Ground-based very low frequency (VLF) radio propagation in the Earth-ionosphere waveguide has enabled extensive electron number densities in the *D* region of the Earth's ionosphere to be determined, by day typically below heights of 70-80 km and by night in the height range ~75-90 km. Many rocket-based electron density measurements have also been reported in the literature from ~60 km upwards using current probes, and radio propagation at a few MHz between the rocket and ground. Recently these rocket measurements have been summarized, and supplemented with *D* region production-loss modeling, giving rise to a near global model named FIRI-2018 (Faraday-International Reference Ionosphere) which provides electron number densities as functions of height, latitude (<60°), solar zenith angle and F10.7 cm solar flux. These rocket-based electron density values are here compared with corresponding values from VLF measurements, by day at a low-latitude (~20°) and a high mid-latitude (~55°), and by night mainly at mid-latitudes. At night the average agreement (over 75-90 km) is remarkably good. By day, at low latitude the agreement is also fairly good (in the common height range ~60-75 km), with the changes with solar zenith angle being moderately comparable. For daytime high mid-latitudes, the agreement is less satisfactory, particularly at the lowest common altitudes, with the VLF measurements showing the expected effects of cosmic rays much more than the rocket-based values. Overall, we find that the *D* region description in the FIRI-2018 model is a significant advance on the earlier International Reference Ionosphere (IRI-2016) model.

1. Introduction

The *D* region is the lowest part of the Earth's ionosphere, found at heights below ~90 km. In quiet times, at non-polar latitudes, its free electrons normally extend down to ~75 km by night and down to ~55 km by day. Production of electrons by day is typically dominated by ionization of the minor atmospheric constituent nitric oxide (NO) by direct solar Lyman-α radiation above ~65-70 km, and by cosmic galactic rays ionizing all neutral constituents below this height. At night, the most significant ionizing source is likely to be the indirect solar Lyman-α reradiated by the neutral hydrogen in the Earth's geocorona (Banks & Kockarts, 1973). Production is essentially balanced by recombination and loss processes. However, these latter processes are not yet sufficiently well understood to enable calculation of reliable absolute electron number densities, and so measurements are needed to create empirical *D* region ionization models. At these low (*D* region) heights, satellite measurements are not practical because the air density is too high creating too much drag, while the electron number densities are normally too low ($10^6 – 10^9$ m^{-3}) to allow sufficient reflection with a conventional ionosonde or an incoherent scatter radar. Two techniques have dominated experimental electron number density measurements in the *D* region at least at non-polar latitudes: (1) ground-based very low frequency (VLF) radio propagation and (2) in situ rocket measurements.

The VLF radio propagation technique has typically used frequencies in the range ~10-40 kHz radiated by powerful (and expensive) ground-based transmitters with very large antennas run by the local military (to communicate with their submarines near world-wide). The receivers are normally rather inexpensive with small (~1-10 m) antennas recording amplitude and phase often continuously, and sometimes are fully portable. The propagation used is in the Earth-ionosphere waveguide where the lower boundary is the ground, or preferably the sea, while the upper boundary is the *D* region of the ionosphere from which the VLF radio waves undergo partial reflection. While the propagation paths over the surface of the Earth can be several thousand km or more, shorter paths of a few hundred km are often more suitable for studying the *D* region in a desired location (e.g., low latitude, mid-latitude etc.). In particular, at a range of ~300-400 km from the transmitter, there is often a 'modal-minimum' where the received amplitude has a marked minimum compared with neighboring ranges; this can be thought of either as waveguide modes interfering or as due to the ground wave from the transmitter interfering with (mainly) the first hop of the transmitter wave reflecting from the *D* region (e.g., Watt, 1967).

In this short path VLF situation, two different sub-techniques have been used. In the first of these, the local geography allowed amplitude and phase to be measured as functions of range over several tens of km near the modal minimum (Thomson et al., 2017). In the second sub-technique, the amplitude and phase were measured both near (<~100 km) the transmitter (where the ground wave is dominant and the ionospheric reflection is near negligible) and at ~300 km from the transmitter (near the modal minimum), where there is good sensitivity to the ionospherically reflected signal (e.g., Thomson et al., 2014). Both these sub-techniques avoid needing to otherwise know the transmitter's radiated power and, in particular, needing to otherwise know the radiated phase of the signal at the transmitter. They are both effectively measuring the changes in phase and amplitude with distance which are then compared with the corresponding calculated changes from the US Navy modal codes, ModeFinder (Morfitt & Shellman, 1976) or LWPC (Ferguson & Snyder, 1990; see also Ferguson,

1998) using a range of possible model electron number densities versus height to find the one that best fits the experimental observations. Both phase and amplitude comparisons are normally essential for VLF ionospheric measurements to avoid ambiguity and achieve good accuracy and reliability.

In contrast, the rocket measuring technique (e.g., Friedrich et al., 2018) involves transmitting an MF (medium frequency) linearly polarized radio wave of a few MHz usually (nowadays) from the ground for reception on the rocket where its received polarization is measured as the height of the rocket changes. This is aided by the rocket spinning at a slow but known rate about its vertical axis. The transmitted linearly polarized wave can be thought of as being made up of two equal right and left circularly polarized waves. Once these enter the plasma (i.e., where there are free electrons in the ionosphere) these two travel as separate modes with different phase velocities and attenuations. This means that when they ‘recombine’ (i.e., are measured together on the rocket) their combined (quasi-linear) polarization will be found to have rotated by an amount related to the amount of plasma the waves have passed through (Faraday rotation) while the extent of the ellipticity of the received polarization is a measure of the relative attenuation of the two polarization modes (right and left) which in turn is also a measure of the amount of plasma passed through. Thus the rotating polarization and the changing relative amplitudes measured on the rocket are continuously measuring the plasma changes as the rocket rises (or falls) and so effectively measuring the refractive index and hence electron number density at the current height of the rocket.

Both the ground-based VLF-radio technique and the rocket-based MF-radio technique require the (appropriate) electron-neutral collision frequency at each height to determine the electron number density at that height. This requires the neutral number densities at each height, particularly the nitrogen (N_2) number density since N_2 is ~78% of the neutral atmosphere at and below *D* region heights. Friedrich et al. (2018), when reporting on their rocket-based FIRI-2018 electron density model, used the NRLMSISE-00 model (Picone et al., 2002), being the latest neutral atmosphere model then available. For the VLF data used here, we use the newer NRLMSIS 2.0 model (Emmert et al., 2020). VLF-determined *D* region results are normally reported using the 'Wait' (e.g., Wait & Spies, 1964) height and sharpness parameters H' and β (e.g., Thomson et al., 2014, 2017) to describe the variation with height of the electron number density in the *D* region at the time and location of the VLF measurements. This has been done because these two parameters can be determined largely independently of the neutral density and collision frequency height profiles assumed at the time. Later, as here, when the best values of electron number density at the time and place of the VLF measurements are required (Thomson et al., 2018, 2021) these values can be obtained retrospectively from the measured H' and β, together with the most recent best estimates of the neutral atmospheric density and collision frequency.

In determining the electron densities from the VLF observations here we use the same formula for the monoenergetic electron-neutral collision frequency as used in developing FIRI-2018 – i.e., $\nu_m = Kp$ where p is the pressure at height, h, and $K = 6.4 \times 10^5$, in SI units (Friedrich & Torkar, 1983), with $p = NkT$ being determined from the appropriate NRL atmospheric model, where N is the (total) neutral number density, k is Boltzmann's constant, and T is the neutral temperature. However, as discussed by

Thomson et al. (2018), the available VLF propagation codes, such as ModeFinder and LWPC, use the Appleton-Hartree equations which assume the electron-neutral collision cross section is independent of velocity whereas the rocket-based electron number densities in FIRI-2018 (Friedrich et al., 2018) used the more recent Sen-Wyller equations where the electron-neutral collision cross section is taken as proportional to the electron velocity. This means that the above $\nu_m = Kp$ can be used directly in the Sen-Wyller equations but requires modification before use in converting the VLF-measured H' and β values into electron densities. As also discussed by Thomson et al. (2018), Deeks (1966), using both Appleton-Hartree and Sen-Wyller formulations at VLF, calculated a series of adjustment factors between 1.5 and 2.5, starting with 1.5 low in the *D* region and increasing monotonically to 2.5 high in the *D* region by which ν_m should be increased to generate an effective ν for use in Appleton-Hartree formulations to give as near as possible the same results as the Sen-Wyller formulation. Thus, as recommended by Deeks (1966), we have here used this appropriate factor at each height as plotted in his figure 1a.

As discussed in Thomson et al. (2018), Wait and Spies (1964) defined the parameter $\omega_r = \omega_o^2/\nu$ where ω_o is the angular (electron) plasma frequency, and ν is an appropriate effective collision frequency such as the "effective ν" described towards the end of the previous paragraph. The electron number density is thus given by $N_e \approx \nu\omega_r/3183$ (since $e^2/\varepsilon_o m_e \approx 3183$), and ω_r was taken to vary with height, h, as $\omega_r = 2.5 \times 10^5 \exp(h - H')\beta$ rad/s thus defining H' as the (reference) height at which $\omega_r = 2.5 \times 10^5$ rad/s, and β as a (near) constant with height, but dependent, even in quiet times, on latitude, time of day, and solar cycle.

For our main comparisons here between electron number densities from FIRI-2018 and those from VLF measurements, we have chosen (1) daytime at a low latitude in the Hawaiian Islands, latitude ~20° N, using transmitter NPM on 21.4 kHz, (2) daytime at a high mid-latitude from the 23.4 kHz transmitter DHO in north Germany (a) along the west coast of Denmark's Jutland peninsula and (b) across the North Sea to Eskdalemuir, Scotland, both at latitudes ~55° N, and (3) nighttime at mid-latitudes, all at relatively quiet times. The VLF phase and amplitude measurements were made using both a (hand-held) portable loop receiver for daytime observations, and at least one (usually more) separate fixed receivers recording continuously. All phases were referenced to one-second pulses from GPS (the satellite Global Positioning System). The fixed recorders enabled any phase or amplitude changes which occurred at the transmitters to be corrected for. Details can be found in Thomson et al. (2014, 2017, 2018, 2021) and references therein. No polar comparisons are made because FIRI-2018 does not extend higher than ~60° latitude. Recently Siskind et al. (2018) compared some daytime VLF-derived electron number densities with those from rocket soundings but did not make any detailed comparisons with the FIRI-2018 model.

FIRI-2018 is available as 1980 profiles of electron number densities between 60 and 150 km altitude, including 11 solar zenith angles 0°, 30°, 45°, 60°, 75°, 80°, 85°, 90°, 95°, 100° and 130°, 5 latitudes 0°, 15°, 30°, 45°and 60°, three solar activities, F10.7 = 75, 130 and 200 sfu, and for the middle of each calendar month (i.e., a total of $11 \times 5 \times 3 \times 12 = 1980$ profiles). These model profiles are available from https://figshare.com/s/357cb03b3e5bed649bbc (Friedrich et al., 2018) or https://figshare.com/search?q=FIRI-2018 The profiles are actually provided from 55 km to 150 km, at 1 km intervals, but Friedrich et al. (2018) advise that they consider them reliable only above 60 km (and for electron densities larger than 10^6 m^{-3}). Recently Xu et al. (2021) have reported on parameterizing (fitting) each of these 1980 FIRI-2018 electron density profiles with Wait and Spies (H' and β) parameters. These could then potentially be used to compare with the corresponding VLF-derived Wait and Spies parameters. However, we prefer here to compare electron density height-profiles from VLF with those from FIRI-2018.

2. Daytime Low-Latitude Comparisons: VLF and FIRI-2018

The VLF results used here are those from August 2012 reported by Thomson et al. (2014).

2.1 Comparisons near Midday at Solar Zenith Angle ~10º

The VLF measurements made in August 2012 in Hawaii (latitude 20.5ºN) described in Thomson et al. (2014) showed that near noon when the solar zenith angle was ~10º that the *D* region was characterized by the Wait parameters H' =69.3 km and β = 0.49 km^{-1}. These parameters lead to the electron number densities shown by the (nearly) straight black line with large open '+' plot symbols in the upper panel of Figure 1. These were calculated using the formula $N_e = \nu\omega_r/3183$ from section 1 above where the (Deeks-adjusted) collision frequency, ν, was derived, as also explained in section 1, from the NRLMSIS 2.0 neutral densities for the time and location of the measurements, thus representing the best estimate of the electron densities from these VLF observations (i.e., using H' =69.3 km and β = 0.49 km^{-1}).

The four curves to the left of the black VLF line are the appropriate FIRI-2018 (Friedrich et al., 2018) electron number density profiles for comparison, e.g., in the label “M8X30L15F130”, M8 means Month 8 = August, X30 means a solar zenith angle of 30º (‘Chi’ in FIRI-2018), L15 means latitude 15º, F130 means F10.7 = 130 solar flux units, etc. So, three of these four curves are for solar zenith angles of 0° which are likely to be the nearest match to the actual 10°, and the other at 30° is for comparison. The upper orange horizontal line is at H' =69.3 km, above which height the VLF measurements are essentially insensitive to the electron number density (e.g., Siskind et al., 2018). This insensitivity above height, H', applies at least as low as H' ≈ 58 km at the peak of an X6 flare (McRae & Thomson, 2004). The lower orange horizontal line at 60 km is the height above which Friedrich et al. (2018) state that their FIRI-2018 electron number densities are considered ‘reliable’. As can be seen the agreement between the VLF and FIRI-2018 electron number densities is good near the center of the height range (64-67 km) where both sets of densities are valid, but at both the lower and upper limits of the mutual height range validity (~60 km and 69 km) the FIRI 2018 values are lower than the VLF values by a not insignificant factor of ~1.6. This will be further considered in section 2.3 below. In particular, below heights of ~62 km, the FIRI and VLF derived electron number densities run nearly parallel with a height difference of ~1 km meaning that the FIRI-2018 values are very similar to a “Wait 70/0.5” profile (H' =70 km and β = 0.5 km^{-1}); this will be commented on again in the next subsection and in section 3 below.

2.2 Comparisons early/late in the day at Solar Zenith Angle ~75º

Thomson et al. (2014) showed that, when the solar zenith angle was ~75º, the low latitude (Hawaiian) *D* region was characterized by the Wait parameters H' =78.6 km and β = 0.29 km^{-1} in the morning (~1730 UT) and H' =77.4 km and β = 0.31 km^{-1} in the afternoon (~0330 UT), giving an am/pm average of H' =78.0 km and β = 0.30 km^{-1} for SZA=75º. These average values lead to the electron number densities shown by the two (nearly) straight lines (on the left) in the middle panel of Figure 1. These blue and red-brown lines with open ‘+’ plot symbols show the electron number densities using the NRLMSIS 2.0 Deeks-adjusted collision frequencies at 1730 and 0330 UT respectively. In this panel, the 4 curves to the right are the FIRI-2018 electron number densities in August at a solar zenith angle of 75º at the two latitudes of 15º and 30º and at the two F10.7 values of 75 and 130 sfu (similar to the top panel). Also, rather similar to the top panel, the FIRI electron number densities at the lowest heights again run from ~2×10^6 m^{-3} at 55 km to ~2×10^7 m^{-3} at 62 km, i.e., are rather similar to a “Wait 70/0.5” profile (H' =70 km and β = 0.5 km^{-1}); this will be commented on again in section 3 below.

The lower orange horizontal line remains at 60 km in the lower panel because this is the Friedrich et al. (2018) FIRI-2018 lowest height of ‘reliability’; the upper orange line is now at 78 km because this is ~*H’* at the SZA of 75º and is thus the greatest height at which the VLF measurements are sensitive to the electron number density. Overall, the agreement between VLF and FIRI-2018 at SZA=75º is neither good nor bad; it is, however, quite passable. More discussion on this is given in the next sub-section.

2.3 VLF Phase & Amplitude Calculated with FIRI Compared with Observations

Instead of entering values of H' and β, ModeFinder allows entry of an electron density versus height profile and a collision frequency versus height profile which are then used to find the appropriate VLF modes under these supplied *D* region characteristics; from these, ModeFinder calculates the amplitude and phase of the signal at the receiver (in a very similar way to when H' and β are supplied as inputs). The FIRI-2018 electron density profiles for August for latitudes 0º, 15º and 30º were used here.

A simple quadratic interpolation was used at each height (1 km intervals) to find the "FIRI-2018" profile for latitude 20.5º (the latitude of the NPM-Hawaii path). This was done for each of the nine (FIRI-2018 tabulated) solar zenith angles between 0º and 95º, and for each of the two tabulated solar activities, F10.7 = 75 and 130 sfu. The collision frequency profile was generated from the NRLMSIS 2.0 neutral density profile, at latitude 20.5º, using the Deeks adjustment as above. The midday collision frequency profile so generated was used for all 9 solar zenith angles because, at this low latitude, the effect on the calculated phases and amplitudes of using more exact timing was found to be negligible. The results are plotted in Figure 2 with the phases shown in the upper panel and the amplitudes shown in the lower panel. The means of the two F10.7 values (75 and 130 sfu) are also shown, as F10.7 = 102 sfu which is close to the actual value of F10.7 at the time of the VLF observations (August, 2012). Also shown are the best-fit curves for the VLF phases and amplitudes versus solar zenith angle actually observed for both morning and afternoon from Thomson et al. (2014). The FIRI-2018 model does not differentiate between morning and afternoon; it specifies only the solar zenith angle.

As can be seen, in both the phase and amplitude panels of Figure 2, there is clearly some agreement between the observed values as functions of solar zenith angle and those calculated from the FIRI-2018 model at least in general shape, apart from the highest solar zenith angles (90º-95º). For low solar zenith angles (~10º, near midday), there is a fairly significant difference with the FIRI-2018 calculated phase value of ~55º being higher than that observed by ~25º. From the upper panel of Figure 2, it can be seen the observed phase does not reach 55º until the solar zenith angle is 35º-40º. From Thomson et al. (2014), using their figure 3 or 5, this implies the FIRI-2018 profile is ~0.8 km higher than the VLF profile (H' = 69.3 km) agreeing, at least approximately, with the apparent relative heights of the VLF and FIRI-2018 profiles shown in the upper panel of Figure 1 here.

3. Daytime High Mid-Latitude Comparisons: VLF and FIRI-2018

The VLF results used in this section are from July 2015 as reported by Thomson et al. (2017), using two closely located, high mid-latitude paths from DHO in north Germany (1) along the west coast of Jutland, Denmark and (2) across the North Sea to Eskdalemuir in Scotland.

3.1 Comparisons near Midday at Solar Zenith Angle ~33º

The VLF measurements made in July 2015 from north Germany to Denmark (latitude ~54.5ºN) of Thomson et al. (2017) showed, near noon when the solar zenith angle was ~33º, that the *D* region was characterized by the Wait parameters H' = 72.8 km and β = 0.345 km^{-1}. These parameters lead to the electron number densities shown by the (nearly) straight black line with large open '+' plot symbols in the upper panel of Figure 3, calculated using the formula $N_e = \nu\omega_r/3183$ with the (Deeks-adjusted) collision frequency, ν, being derived from NRLMSIS 2.0 neutral densities for the time and place of the measurements. To the left, the four colored curves show for comparison the corresponding FIRI-2018 electron number density profiles for latitudes near 55º N at solar zenith angles of 30º and 45º, in July 2015 when F10.7 = 130 sfu.

At the greatest heights at which the VLF measurements are sensitive (~72.8 km, ~ H'), it can be seen, in the upper panel of Figure 3, that the agreement is quite good between the VLF-derived electron densities (at ~55º latitude) and the FIRI-2018 model at a solar zenith angle of ~33º and a latitude of 45º (FIRI data "M7X30L45F130"); however, as can also be seen, the FIRI model gives somewhat lower electron densities at the higher latitude of 60º. Although this overall agreement at heights near 72 km is quite passable, it is also clear that towards the lowest heights (~60 km) at which the FIRI model is considered reliable (Friedrich et al., 2018), its electron densities are significantly lower (by a factor of nearly 3) than the VLF-derived values. In particular, the FIRI electron densities at a height of 60 km are nearly the same ($\sim 1.0 \times 10^7$ m^{-3}) at latitude 20º (as shown in Figure 1) and at latitudes ~55º shown here, whereas the ionization due to galactic cosmic rays is expected to be significantly higher at these higher latitudes (e.g., Heaps, 1978).

3.2 Comparisons early/late in the day at Solar Zenith Angle ~75º

The same set of VLF measurements reported by Thomson et al. (2017), from July 2015 at latitude ~54.5º N, in section 3.1 above, but using the path DHO to Eskdalemuir instead of DHO to Denmark, showed that at solar zenith angles of ~75º the *D* region was characterized by H' = 76.6 km and β = 0.27 km^{-1}; these parameters lead to the electron number densities shown in the lower panel of Figure 3 by the two fairly similar nearly straight lines (to the right), with open '+' plot symbols, again using the formula $N_e = \nu\omega_r/3183$ as above. Both these lines use NRLMSIS 2.0 but the blue line is for 6 UT (morning) while the red-brown line is for 18 UT (afternoon) to illustrate the small but noticeable difference. The FIRI model does not discriminate between morning and afternoon so such differences are not pursued further here. Again it needs to be noted that all the FIRI profiles in all four panels of Figures 1 and 3 are essentially the same at ~60 km and below, independent of latitude.

As can be seen in this lower panel of Figure 3, at the greatest heights at which the VLF measurements are sensitive (*H'* ~ 76 km) the FIRI-2018 electron densities, for a solar zenith angle of 75º are low (plot symbol squares, ~1.1×10^8 m^{-3}) by a factor of ~2 compared with the VLF results. However, if FIRI electron densities at a solar zenith angle of 60º (not shown) were used instead the agreement would be much better, being then just marginally higher (~2.5×10^8 m^{-3} at 76 km) than the VLF results. This might possibly be due to a scarcity of rocket profiles (in solar zenith angle and latitude).

Again, as in section 3.1, it is clear that towards the lowest heights (~60 km) at which the FIRI model is considered reliable its electron densities are lower (by a factor ~2.5) than the VLF-derived values. Also, the FIRI electron densities at a height of 60 km are nearly the same (~1.0×10^7 m^{-3}) at latitude 20º (as shown in Figure 1) and at latitudes ~55º shown here, whereas the ionization due to galactic cosmic rays is expected to be significantly higher at these higher latitudes (e.g., Heaps, 1978). Siskind et al. (2018) have also pointed out that sounding rocket profiles have tended to fail to show the increasing electron densities with increasing latitude (at low altitudes) expected from the well-known, corresponding increases in galactic cosmic rays.

3.3 VLF Phase & Amplitude Calculated with FIRI Compared with Observations

Section 2.3 above used ModeFinder to calculate VLF phases and amplitudes on our low latitude path as functions of solar zenith angle using appropriate low latitude FIRI-2018 electron density profiles, and compared these with the corresponding VLF observations in Figure 2. Here, in Figure 4, similar comparisons are made but for the high mid-latitude path DHO to Eskdalemuir; as can be seen, the agreement between the VLF observations (from Thomson et al., 2017) and the calculations using the appropriate FIRI profiles for both the phases (upper panel) and the amplitudes (lower panel) is relatively poor. A significant contributor to this poor level of agreement is likely to be related to the FIRI-2018 model not fully recognizing a greater number of galactic cosmic ray generated electrons below heights of ~70 km at these relatively high latitudes. While these cosmic ray generated electrons will not themselves vary much with solar zenith angle (during daytime), the electron density above ~70 km is solar generated (mainly Lyman-α) and so solar zenith angle dependent. Whether this effect actually shows up in the VLF phases or amplitudes depends on the exact nature of the path, including its length. Here, as the VLF observations show, the VLF phase is quite strongly solar zenith angle dependent while the amplitude is not.

4. High Mid-Latitude VLF Electron Densities below ~60 km Height

Comparing the two panels of Figure 3, it can be seen that at heights below ~60 km the VLF-derived electron number densities near noon are lower than early or late in the day; e.g., at 55 km specifically, the VLF-derived electron number density at a solar zenith angle of 75º shows $\sim 1.2 \times 10^7$ m^{-3} in the lower panel while at a solar zenith angle of ~33º, in the upper panel, it shows as $\sim 0.9 \times 10^7$ m^{-3}, i.e., ~30% lower. This seems unlikely because galactic cosmic rays, which are the principal ionizing source at these heights, are not solar zenith angle dependent. Another possibility could be the photo-detachment, by visible light at sunrise, of electrons (e.g. Kazil et al., 2003, Ogawa & Shimazaki, 1975) from negative ions generated during the night from galactic cosmic rays, but this effect is likely to have faded when the sun has risen to a solar zenith of 75º (and also does not occur at dusk).

To assess whether this difference is significant in terms of likely errors, the noon profile of H' = 72.8 km and β = 0.345 km^{-1} as determined by Thomson et al. (2017) was compared with a similar profile with two parts, H' = 76.6 km and β = 0.27 km^{-1} (as for a solar zenith angle of 75°) below 60 km and H' = 72.6 km and β = 0.355 km^{-1} above 60 km as shown in the upper panel of Figure 5. The lower two panels of Figure 5 here are taken from Thomson et al. (2017) showing the measured (data points) and calculated (lines) phases and amplitudes versus distance, with the new (ModeFinder) calculated (thick green) lines superposed for the new two-part profile with H' = 72.6 km and β = 0.35 km^{-1} (for phase) and β = 0.36 km^{-1} (for amplitude) above 60 km and H' = 76.6 km and β = 0.27 km^{-1} below 60 km. As can be seen the (previous) best fit black lines (H' = 72.8 km and β = 0.345 km^{-1}) fit the data points just as well as the new green lines. The change of just 0.2 km in H' and 0.01 km^{-1} in β is within the originally estimated experimental error and so is not of much significance.

Of course, instead of adjusting the noon profile below 60 km to the 75° profile, the 75° profile could have been adjusted instead (e.g., by similarly making into two parts) so that, below 60 km it matched the original, H' = 72.8 km and β = 0.345 km^{-1}, noon profile, or indeed both noon and 75° profiles could have each been even more slightly adjusted (in two parts) so that they matched below 60 km. This would involve < 0.2 km in H' and <0.01 km^{-1} in β and so be of near negligible significance. Also new in Figure 5 are orange '+' symbols, identical to the new green profile but with it cut-off at a height just below 57 km, showing that the VLF technique is here sensitive down to heights at least as low as 57 km.

5. Nighttime *D* region Comparisons: VLF and FIRI-2018

The nighttime VLF-derived electron number densities used in this section come from long, nearly all-sea paths over a range of latitudes, but excluding both the polar regions (>~60º latitude, as does FIRI-2018) and the equatorial regions (say <~15º geomagnetic latitude), mainly from Thomson et al. (2007) but also supported by Thomson and McRae (2009). Thomson et al. (2007) found H' = 85.1 ± 0.4 km and β = 0.63 ± 0.04 km^{-1} on average, predominantly in summer and under conditions nearer solar minimum than solar maximum. The FIRI-2018 profiles compared in this section are those with solar zenith angles of 130º (the highest solar zenith angle reported in FIRI-2018) which correspond with being full night. The next highest solar zenith angle available in FIRI-2018 was 100º; it was decided not to use these 100º values for comparisons because they would be only just into full darkness and the VLF data reported in Thomson et al. (2007) was wholly or mainly with solar zenith angles greater than 100º, i.e., with the ionosphere well settled into full night.

Figure 6 compares the VLF-derived nighttime electron number densities with those from FIRI-2018. The thick black solid (nearly) straight line with the open '+' plot symbols shows the VLF-derived electron number densities for H' = 85.0 km and β = 0.65 km^{-1} using collision frequencies derived (as above) from the NRLMSIS 2.0 model (nominally for July at 45º latitude, 0º longitude, and 0 UT, though this was not critical). The solid blue line is similarly calculated for H' = 85.0 km and β = 0.60 km^{-1}. The FIRI-2018 electron number densities are shown with the dot/dashed curves with the plot-symbol labeling similar to that used above except that the 'X130' (indicating a solar zenith angle of 130º) is not shown in the labels because they are all for 130º. So, e.g., 'M7L45F130' means Month 7 (i.e., July), Latitude 45º, solar Flux

130 sfu. The VLF data correspond to solar activity roughly midway between F10.7 solar fluxes of 75-130 sfu. Friedrich et al. (2018) have indicated that FIRI-2018 electron number densities below 1×10^6 m^{-3} are not considered reliable; so these have been included only for completeness. At night (when *H'* ≈ 85 km), ModeFinder calculations show that the VLF technique is sensitive down to heights ~75 km, and up to heights of ~90 km, i.e., somewhat above *H'* (the daytime sensitivity upper height limit mentioned in section 2.1).

In Figure 6, it can be seen that the agreement between the night VLF-derived *D* region electron number densities and those from the (rocket-based) FIRI-2018 model is remarkably good, especially at latitudes near 45º. It must be emphasized that these are all averaged values; the night *D* region is rather variable (e.g., Thomson et al., 2007) in time and space (compared with the daytime *D* region) whether observed by ground-based VLF or by rocket-borne MF radio. In particular, as pointed out by Friedrich et al. (2018), the actual individual nighttime electron density profiles as measured by rockets at a particular place and time often show 'ledges' where the electron density increases much more rapidly with height than shown here in Figure 6, but these ledges occur (randomly) at different heights, typically between ~80-90 km, and so, when averaged, result in the profiles in Figure 6. At night, galactic cosmic rays generate free electrons at similar rates as by day; these electrons are then similarly rapidly removed by attachment to neutral molecular oxygen molecules: $e^- + O_2 \rightarrow O_2^-$. By day, photons of (visible) sunlight immediately release these electrons again from the negative ions, resulting in cosmic ray generated free electrons dominating below heights of 65-70 km as noted above. In darkness, this last step cannot occur, resulting in very few free electrons from cosmic rays at night (Thomson et al., 2021; see also Banks & Kockarts, 1973).

Cummer et al. (1998) and Cheng et al. (2006) used VLF propagation from natural lightning (sferics) to determine nighttime *D* region characteristics over the USA at latitudes ~35º-37º with both also finding $H' \approx 85.0$ km but both finding significantly lower values of β with Cummer et al. finding $\beta \approx 0.50$ km^{-1} and Cheng et al. $\beta \approx 0.45$ km^{-1}.

6. Neutral Atmosphere Collision Effects on VLF Electron Densities

The VLF-derived electron number densities presented in the previous sections here were calculated from their measured H' and β values using the NRLMSIS 2.0 neutral density model (Emmert et al., 2020) as explained in section 1 above. These VLF-derived electron number densities are now compared with (1) those similarly derived from the NRLMSISE-00 model (Picone et al., 2002) as used by Friedrich et al. (2018) for FIRI-2018, and (2) those derived using, as also discussed in section 1, the 'Wait' collision frequency (with collision cross section independent of velocity, and so with no Deeks adjustments) as incorporated in ModeFinder, i.e., $\nu = 5.0\exp(-0.15(h - 70))$ MHz. In Figure 7, the top and middle panels make these comparisons for the low latitude case (~20º N) and the high mid-latitude case (~55º N) respectively, at the two appropriate daytime solar zenith angles (mid-day, 10º and 33º respectively, and 75º), while the bottom panel is for night (at mid-latitudes).

It can be seen that the electron densities using NRLMSISE-00 are normally only very slightly (and so negligibly) larger than those using NRLMSIS 2.0. Only at both higher latitude (~55º N) and higher solar zenith angle (SZA=75º), and at daytime heights >70 km, do the NRLMSISE-00 electron densities become appreciably, though still marginally, larger (by ~10%) than those using NRLMSIS 2.0. In contrast, while the 'Wait'-derived electron densities nearly always deviate from the NRLMSIS 2.0 values more than those from NRLMSISE-00, none-the-less they do not deviate very much for both daytime low latitudes (~20º N) and nighttime mid-latitudes. However, as can be seen in the middle panel, the 'Wait'-derived electron densities at the high mid-latitude of ~55º are typically significantly lower by up to factors of ~1.6, compared with those derived from the more modern collision frequencies and atmospheric models.

7. Comparisons: IRI and VLF

The *D* region part of the FIRI-2018 model is considered a significant advance on the *D* region part of the current (2016) International Reference Ionosphere (IRI-2016) model (Bilitza, 2017). Here we compare the VLF electron number densities with the equivalent IRI-2016 profiles. In the *D* region, IRI-2016 uses IRI-95 which is based on an older and much smaller selection of typical rocket profiles such as those in Mechtly et al. (1972) who also used Langmuir probes calibrated by Faraday and differential-absorption data. The IRI-2016 data used here came from the NASA web page https://ccmc.gsfc.nasa.gov/modelweb/models/iri2016_vitmo.php which also includes a second *D* region model "FT-2001" which is a much earlier version of FIRI (Friedrich & Torkar, 2001). Figure 8 shows comparisons between (1) the VLF-derived electron number densities presented here in sections 2, 3 and 5, and (2) the corresponding IRI data. The top and middle panels are for mid-day at latitudes of ~20º and ~55º respectively, while the bottom panel is for night at mid-latitudes. As can be seen, a principal disadvantage of the IRI-2016 *D* region models is that their electron density profiles do not extend down as low as either the FIRI-2018 or the VLF profiles. By day (upper two panels) the IRI-2016 profiles extend down to ~65 km compared with down to ~60 km for FIRI-2018. This means they are essentially not registering electrons generated by galactic cosmic rays; it also largely precludes their use for VLF modeling such as for the phase and amplitude calculations performed using FIRI-2018 here in sections 2.3 and 3.3. Similarly at night (bottom panel) it can be seen that the IRI-95 and FT-2001 profiles extend down only to 80 and 83 km respectively. Also, although the agreement between the VLF and FT-2001 profiles is good (down to just ~83 km), there is little agreement with IRI-95 profile. In the top panel, even where the red, IRI-95 profile crosses the black VLF line, the IRI-95 line has a slope corresponding to $\beta = \sim 0.40$ km^{-1} while the VLF observations give $\beta = \sim 0.49$ km^{-1} which, as can be seen in figure 3 of Thomson et al. (2014), is quite a large difference (corresponding to 4-5 standard deviations or 4-5 dB in amplitude).

8. Summary and Conclusions

The FIRI-2018 model uses rocket observations and modeling to provide an impressive range of ionospheric electron number densities for heights, in 1-km intervals, from 150 km down to nominally 55 km though only those above 60 km, and >10^6 m^{-3}, are considered reliable (Friedrich et al., 2018). Such profiles are provided at 5 latitudes (0-60º), 11 solar zenith angles, 3 solar activities and for each of 12 months, making a total of 1980 profiles. While a significant amount VLF data exists, this has not yet been sorted comprehensively. We therefore chose to select three representative conditions where extensive quality VLF data were available: nighttime at mid-latitudes, daytime at low latitude (~20º) and daytime towards the higher end of the FIRI-2018 latitudes (~55º). While VLF data can give very good electron number densities, the technique works only in the lowest parts of the Earth's ionosphere. During quiet times this means ~75-90 km altitude by night, ~55-70 km near mid-day at low latitudes, and ~60-75 km at higher solar zenith angles or mid-latitudes. Both the VLF technique and this lowest ionospheric region are none-the-less very important in geophysics. Both man-made and natural (e.g., lightning) VLF radio signals propagate in the Earth-ionosphere waveguide and so are sensitive to the lower *D* region, by day, night, dawn and dusk, both in quiet conditions and when disturbed, such as by energetic electron (or proton) precipitation or by solar flares or by (extra-terrestrial) gamma rays etc. Production and loss modeling in the *D* region is very important in attempting to get a good quantitative understanding of the key mechanisms there. Recently Siskind et al. (2018) found that, by day, their theoretical photochemical model agreed better with VLF-derived electron densities below 68–70 km than the corresponding electron densities from rockets. There appear to be multiple complex processes involved in such *D* region modeling which are likely to result in further developments but need the support of measured electron number densities.

The agreement found here between VLF-derived and FIRI-2018 electron densities is, perhaps surprisingly, best at night. This may be partly because, at night, both techniques have good sensitivity in the height range 75-90 km. The MF rocket sensitivity has a threshold of typically between 10^9 m^{-3} at 60 km and 10^7 m^{-3} at 80 km (Friedrich et al., 2018; Jacobsen & Friedrich, 1979) and so in the relevant height range of 75-90 km the more sensitive but much less certain Langmuir probe data will have been only minimally required, if at all. Also, the lower limit for electron densities of 10^6 m^{-3} (at any height) will have been encountered only below ~75 km. In addition, both techniques will have averaged out any of the "ledges" mentioned here in section 5: VLF by averaging over long paths and by averaging over several days, and FIRI-2018 by averaging over a number of rocket profiles.

For daytime low latitudes (~20º), the agreement found here between VLF-derived and FIRI-2018 is quite reasonable, specifically for the electron densities at the solar zenith angles of ~10º and ~75º and more generally in terms of the agreement between observed and ModeFinder+FIRI-2018 predicted VLF phases and amplitudes as functions of solar zenith angle. It might well be fair to say that probably from the very general, global perspective of the FIRI-2018 model, the agreement is quite good, while from the highly focused VLF perspective, the agreement is more modest.

For daytime high mid-latitudes (~55º), the degree of agreement found here between VLF-derived and FIRI-2018 is at best only quite modest, with the FIRI-2018 densities being consistently lower by up to a factor of ~3 than the VLF-derived values. Again, it might well be fair to say that probably from the very general, global perspective of the FIRI-2018 model, the agreement is generally passable while, from the highly focused VLF perspective, the agreement is fairly marginal. A significant factor, at these higher latitudes in daytime, may well be that FIRI-2018, at the lowest altitudes, in compromising between the rocket (probe, rather than MF) observations and modeling, has perhaps underestimated the galactic cosmic ray generated electrons. In contrast, the FIRI-2018 profiles at low latitude (20º) and high solar zenith angle (75º), in the middle panel of Figure 1, show an electron density 'bulge' at ~65 km, which appears consistent with cosmic ray generated electrons, below a 'dip' at 70 km down to which height Lyman-α is likely no longer penetrating at this high solar zenith angle.

Although, as mentioned above, the FIRI-2018 model does not extend above latitudes ~60º, comparisons of VLF-derived electron densities in polar regions with those from sounding rocket profiles and an MF radar have shown them to be quite comparable both by day and by night (Thomson et al. 2018, 2021).

Overall, our comparisons here with specific VLF-derived electron number densities indicate that the FIRI-2018 model, though under-estimating at higher latitudes by day, is a major advance at least compared with IRI-2016. We conclude that FIRI-2018 reasonably represents the *D* region electron number density profiles on a near global basis (i.e., at latitudes below 60º), at least in the low height ranges where it can be compared with VLF measurements.

Data Availability Statement

The NRLMSIS 2.0 neutral atmospheric data were obtained using the FORTRAN code at https://map.nrl.navy.mil/map/pub/nrl/NRLMSIS/NRLMSIS2.0/ but should also be available from https://kauai.ccmc.gsfc.nasa.gov/instantrun/msis

The NRLMSISE-00 neutral atmospheric data were obtained from the NRLMSISE-00 web model at https://ccmc.gsfc.nasa.gov/modelweb/models/nrlmsise00.php but should also be available from https://kauai.ccmc.gsfc.nasa.gov/instantrun/msis

The FIRI-2018 model profiles are available from https://figshare.com/s/357cb03b3e5bed649bbc (Friedrich et al., 2018) or https://figshare.com/search?q=FIRI-2018

The VLF data used here came from Thomson et al. (2007, 2014, 2017).

US Navy code LWPC is available at https://github.com/mlhutchins/LWPC

The US Navy computer program referred to here as ModeFinder is a slightly modified version of MODEFNDR (e.g., Thomson, 1993; Nunn & Strangeways, 2000) and MODESRCH described and listed in Morfitt & Shellman (1976).

Solar zenith angles were determined at https://gml.noaa.gov/grad/solcalc/

The IRI data used here came from the NASA web page: https://ccmc.gsfc.nasa.gov/modelweb/models/iri2016_vitmo.php

Acknowledgements

Many of the VLF observations used here were supported by funding from the UK Research and Innovation (UKRI-NERC) through National Capability – Space Weather Observatory.

Figure Captions

Figure 1. Low latitude (~20º N) comparisons of VLF-derived (using 21.4 kHz) and FIRI-2018 electron number densities as functions of height. (Top panel) At solar zenith angles ~10º. (Middle panel) At solar zenith angles ~75º. (Bottom panel) Illustrates FIRI-2018 plot symbol labels such as "M8X75L30F130". VLF plot symbol labels such as "69.3/0.49 NRL2.0" mean H' =69.3 km and β=0.49 km^{-1}, and NRL2.0 means the NRLMSIS 2.0 neutral atmosphere model was used to determine the collision frequencies.

Figure 2. VLF phases and amplitudes, as functions of solar zenith angle, observed and calculated for the short (306-km), nearly all-sea, low latitude path from NPM (21.4 kHz) in Hawaii. The thick dashed lines are the observations (from Thomson et al., 2014), light blue for morning and dark red for afternoon. The green, black and red data points, joined by lines of the same colors, were calculated with ModeFinder using the corresponding FIRI-2018 profiles (interpolated for latitude and F10.7 as appropriate – see text for details).

Figure 3. High mid-latitude (~55º N) comparisons of VLF-derived (using 23.4 kHz) and FIRI-2018 electron number densities as functions of height. Plot symbol labels are explained in Figure 1 above. (Top panel) Comparisons at solar zenith angles ~33º. (Bottom panel) Comparisons at solar zenith angles ~75º.

Figure 4. VLF phases and amplitudes, as functions of solar zenith, observed and calculated for the 748-km nearly all-sea, high mid-latitude path, from DHO (23.4 kHz) to Eskdalemuir. The observations (from Thomson et al., 2017) are shown in

light blue for morning and dark red for afternoon. The green and bright red data points, joined by lines of the same colors, were calculated with ModeFinder using the corresponding FIRI-2018 profiles.

Figure 5. Assessing small shape changes in the noon, high mid-latitude, VLF-derived electron density profile. (Top panel) The original (black) H' =72.8 km and β= 0.345 km^{-1} profile from Thomson et al. (2017) together with the new (green) two-part profile as labeled. (Lower two panels) ModeFinder calculations (green lines) for the new profile overlaid on the phase and amplitude observations for 5-17 July 2015 (data points), and calculations (lines) first presented in Thomson et al. (2017) for the high mid-latitude path at noon.

Figure 6. Nighttime, broadly mid-latitude comparisons of VLF-derived and FIRI-2018 electron number densities as functions of height. Plot symbol labels are explained in Figure 1. The VLF technique is not sensitive here above heights of ~90 km. The FIRI electron densities are not considered reliable below densities of 10^6 m^{-3}**.**

Figure 7. VLF-derived electron number densities compared depending on the neutral atmospheric model and so the electron-neutral collision frequencies. SZA = Solar Zenith Angle. (top panel) daytime, latitude ~20º N (Hawaii, August 2012). (middle panel) daytime, latitude ~55º N (North Sea, July 2015). (bottom panel) night, mid-latitude.

Figure 8. VLF-derived electron number densities compared with those from the International Reference Ionosphere, IRI-2016. Comparisons are with each of the two

D region components of IRI-2016: IRI-95 and FT-2001 discussed in the text. (Top panel) Daytime at low latitudes (~20º N**).** (Middle panel) Daytime at high mid-latitudes (~55º N**).** (Bottom panel) Nighttime at mid-latitudes.

References

Banks, P. M., & Kockarts, G. (1973). *Aeronomy*, New York, NY: Academic.

Bilitza, D., Altadill, D., Truhlik, V., Shubin, V., Galkin, I., Reinisch, B., & Huang, X. (2017). International Reference Ionosphere 2016: From ionospheric climate to real-time weather predictions, *Space Weather, 15*, 418–429. https://doi.org/10.1002/2016SW001593

Cheng, Z., Cummer, S. A., Baker, D. N., & Kanekal, S. G. (2006). Nighttime *D* region electron density profiles and variabilities inferred from broadband measurements using VLF radio emissions from lightning, *Journal of Geophysical Research: Space Physics*, *111*(A5), https://doi.org/10.1029/2005JA011308

Cummer, S. A., Inan, U.S. & Bell, T. F. (1998). Ionospheric *D* region remote sensing using VLF radio atmospherics, *Radio Science, 33*(6), 1781-1792. https://doi.org/10.1029/98RS02381

Deeks, D. G. (1966). Generalised full wave theory for energy-dependent collision frequencies. *Journal of Atmospheric and Terrestrial Physics, 28*, 839-846. https://doi.org/10.1016/S0021-9169(17)30005-3

Emmert, J. T., Drob, D. P., Picone, J. M., Siskind, D. E., Jones, M. Jr., Mlynczak, M. G., et al. (2020). NRLMSIS 2.0: A whole - atmosphere empirical model of temperature and neutral species densities. *Earth and Space Science*, 7, e2020EA001321. https://doi.org/ 10.1029/2020EA001321
https://map.nrl.navy.mil/map/pub/nrl/NRLMSIS/NRLMSIS2.0/
https://kauai.ccmc.gsfc.nasa.gov/instantrun/msis

Ferguson, J. A., & Snyder, F. P. (1990). *Computer programs for assessment of long wavelength radio communications, version 1.0: Full FORTRAN code user's guide, Naval Ocean Systems Center Tech. Doc. 1773, DTIC AD-B144 839, Def. Tech. Inf. Cent.*, Alexandria, Va.

Ferguson, J. A. (1998). *Computer programs for assessment of long-wavelength radio communications, version 2.0: User's guide and source files.* SPAWAR Technical Document 3030, San Diego, CA: Space and Naval Warfare Systems Center. https://apps.dtic.mil/sti/pdfs/ADA350375.pdf

Friedrich, M., & Torkar, K.M. (1983). Collision frequencies in the high latitude *D*-region, *Journal of Atmospheric and Terrestrial Physics, 45(4)*, 267-271. https://doi.org/10.1016/S0021-9169(83)80048-8

Friedrich, M., & Torkar, K. M. (2001). FIRI: A semiempirical model of the lower ionosphere. *Journal of Geophysical Research*, *106*(A10), 21409-21418. https://doi.org/10.1029/2001JA900070

Friedrich, M., Pock, C., & Torkar, K. (2018). FIRI-2018, an updated empirical model of the lower ionosphere. *Journal of Geophysical Research: Space Physics, 123*(8), 6737–6751. https://doi.org/10.1029/2018JA025437

Heaps, M. G. (1978). Parameterization of the cosmic ray ion-pair production rate above 18 km. *Planetary and Space Science*, *26*, 513-517. https://doi.org/10.1016/0032-0633(78)90041-7

Jacobsen, T. A., Friedrich, M. (1979). Electron density measurements in the lower *D*-region. *Journal of Atmospheric and Terrestrial Physics, 41*(12), 1195-1200. https://doi.org/10.1016/0021-9169(79)90022-9

Kazil, J., Kopp, E., Chabrillat, S., & Bishop, J. (2003) The University of Bern Atmospheric Ion Model: Time-dependent modeling of the ions in the mesosphere and lower thermosphere. *Journal of Geophysical Research,* 108(D14), 4432-4446. https://doi.org/10.1029/2002JD003024

McRae, W. M., & Thomson, N. R. (2004). Solar flare induced ionospheric D-region enhancements from VLF phase and amplitude observations, *Journal of Atmospheric and Solar-Terrestrial Physics, 66*(1), 77-87. https://doi.org/10.1016/j.jastp.2003.09.009

Mechtly, E. A., Bowhill, S. A., & Smith, L. G. (1972), Changes of lower ionosphere electron concentrations with solar activity. *Journal of Atmospheric and Terrestrial Physics, 34*(11), 1899–1907. https://doi.org/10.1016/0021-9169(72)90065-7

Morfitt, D. G., & Shellman, C. H. (1976). "MODESRCH", an Improved Computer Program For Obtaining ELF/VLF/LF Mode Constants in an EarthIonosphere Waveguide (Naval Electr. Lab. Cent. Interim Rep. 77T, NTIS Accession ADA032573). Springfield, VA: National Technical Information Service. https://apps.dtic.mil/sti/pdfs/ADA032573.pdf

Nunn, D., & Strangeways, H. J. (2000). Trimpi perturbations from large ionisation enhancement patches (LIEs), *Journal of Atmospheric and Terrestrial Physics*, 62(3), 189–206. https://doi.org/10.1016/S1364-6826(00)00004-3

Ogawa, T., Shimazaki, T. (1975) Diurnal variations of odd nitrogen and ionic densities in the mesosphere and lower thermosphere: Simultaneous solution of photochemical-diffusive equations. *Journal of Geophysical Research,* 80(28), 3945-3960. https://doi.org/10.1029/JA080i028p03945

Picone, J. M., Hedin, A. E., Drob, D. P. & Aikin, A. C. (2002). NRLMSISE-00 empirical model of the atmosphere: Statistical comparisons and scientific issues, *Journal of Geophysical Research: Space Physics, 107*(12), 1468-1483. https://doi.org/10.1029/2002JA009430

Siskind, D. E., Zawdie, K. A., Sassi, F., Drob, D. P., & Friedrich, M. (2018). An intercomparison of VLF and sounding rocket techniques for measuring the daytime *D* region ionosphere: Theoretical implications. *Journal of Geophysical Research: Space Physics, 123*(10), 8688–8697. https://doi.org/10.1029/2018JA025807

Thomson, N. R. (1993). Experimental daytime VLF ionospheric parameters. *Journal of Atmospheric and Terrestrial Physics,* 55(2), 173–184. https://doi.org/10.1016/0021-9169(93)90122-F

Thomson, N. R., Clilverd, M. A., & McRae, W. M. (2007). Nighttime ionospheric *D* region parameters from VLF phase and amplitude. *Journal of Geophysical Research*, *112*(A7). https://doi.org/10.1029/2007JA012271

Thomson, N. R., & McRae, W. M. (2009). Nighttime ionospheric *D* region: Equatorial and Non-equatorial, *Journal of Geophysical Research*, *114*(A8). https://doi.org/10.1029/2008JA014001

Thomson, N. R., Clilverd, M. A., & Rodger, C. J. (2014). Low-latitude ionospheric *D* region dependence on solar zenith angle. *Journal of Geophysical Research: Space Physics 119*(8). https://doi.org/10.1002/2014JA020299

Thomson, N. R., Clilverd, M. A., & Rodger, C. J. (2017). Midlatitude ionospheric *D* region: Height, sharpness, and solar zenith angle. *Journal of Geophysical Research: Space Physics*, *122*(8), 8933-8946. https://doi.org/10.1002/2017JA024455

Thomson, N. R., Clilverd, M. A., & Rodger, C. J. (2018). Quiet daytime Arctic ionospheric *D* region. *Journal of Geophysical Research: Space Physics, 123*, 9726–9742. https://doi.org/10.1029/2018JA025669

Thomson, N. R., Clilverd, M. A., Brundell, J. B., & Rodger, C. J. (2021). Quiet night Arctic ionospheric *D* region characteristics. *Journal of Geophysical Research: Space Physics, 126*, e2020JA029043. https://doi.org/10.1029/2020JA029043

Xu, W., Marshall, R. A., Bortnik, J., & Bonnell, J. W. (2021). An electron density model of the D- and E-region ionosphere for transionospheric VLF propagation. *Journal of Geophysical Research: Space Physics*, *126*, e2021JA029288. https://doi.org/10.1029/2021JA029288

Wait, J. R., & Spies, K. P. (1964). Characteristics of the Earth-ionosphere waveguide for VLF radio waves. *NBS Tech. Note 300*, Natl. Bur. of Stand., Boulder, Colo. https://www.govinfo.gov/app/details/GOVPUB-C13-1fc83a916d87542f34917847f89b9f0b

Watt, A. D. (1967). *VLF Radio Engineering.* Oxford: Pergamon Press.

xxx

Figure 1.

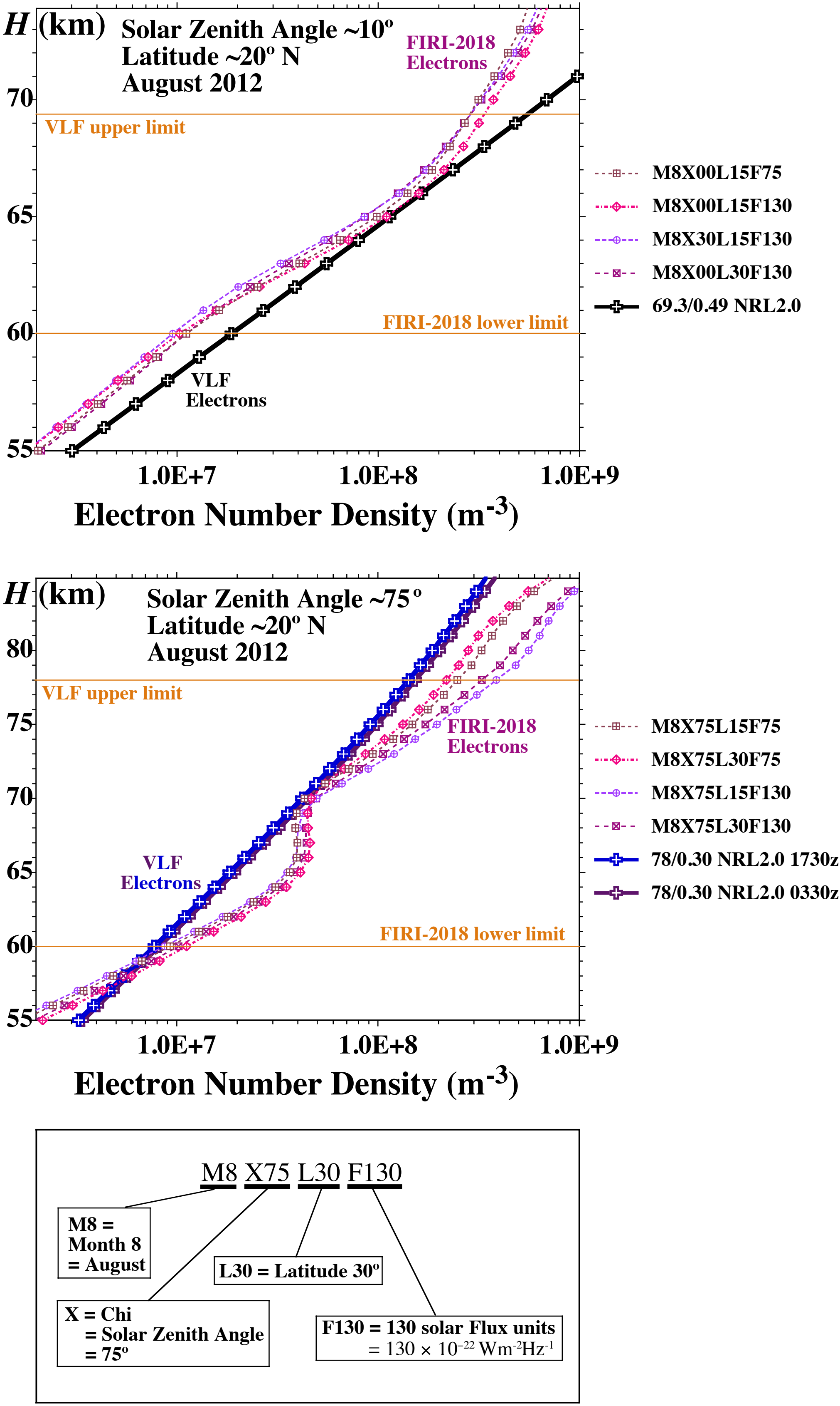
H (km)
Solar Zenith Angle ~10°
Latitude ~20° N
August 2012
FIRI-2018
Electrons
VLF upper limit
FIRI-2018 lower limit
VLF
Electrons
70
65
60
55
1.0E+7
1.0E+8
1.0E+9
Electron Number Density (m-3)
M8X00L15F75
M8X00L15F130
M8X30L15F130
M8X00L30F130
69.3/0.49 NRL2.0
H (km)
Solar Zenith Angle ~75°
Latitude ~20° N
August 2012
VLF upper limit
FIRI-2018
Electrons
VLF
Electrons
FIRI-2018 lower limit
80
75
70
65
60
55
1.0E+7
1.0E+8
1.0E+9
Electron Number Density (m-3)
M8X75L15F75
M8X75L30F75
M8X75L15F130
M8X75L30F130
78/0.30 NRL2.0 1730z
78/0.30 NRL2.0 0330z
M8 X75 L30 F130
M8 = Month 8 = August
L30 = Latitude 30°
X = Chi = Solar Zenith Angle = 75°
F130 = 130 solar Flux units = 130 × 10-22 Wm-2Hz-1

Figure 2.

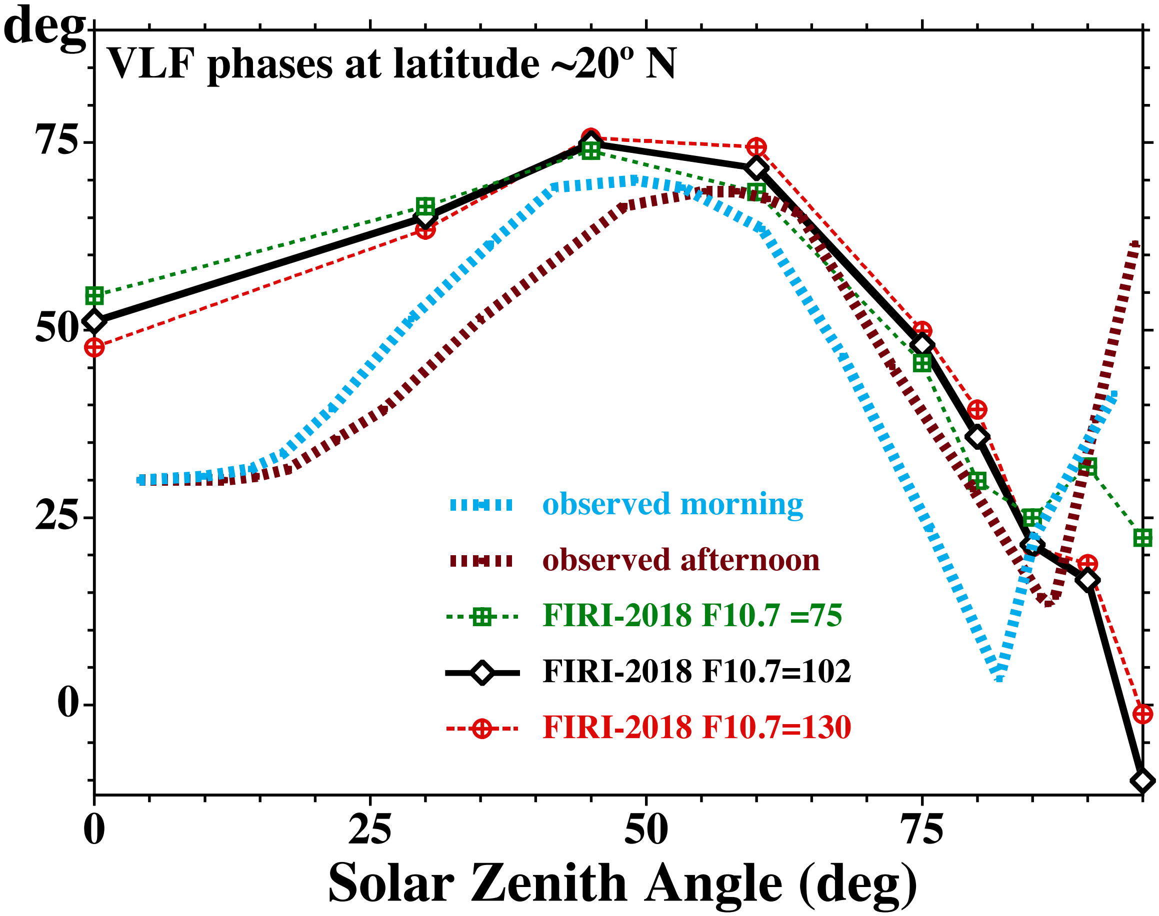
deg
VLF phases at latitude ~20° N
75
50
25
0
observed morning
observed afternoon
FIRI-2018 F10.7 =75
FIRI-2018 F10.7=102
FIRI-2018 F10.7=130
0
25
50
75
Solar Zenith Angle (deg)

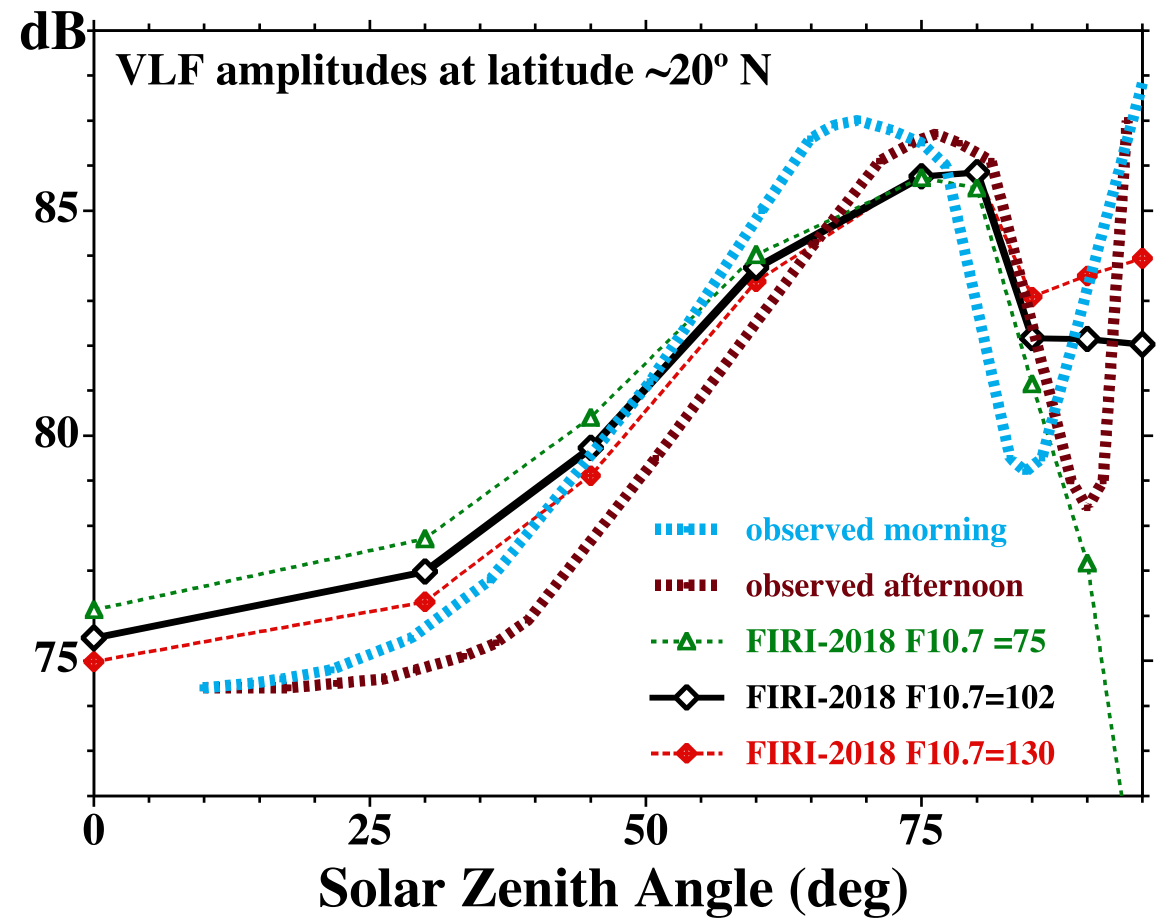
dB
VLF amplitudes at latitude ~20° N
85
80
75
observed morning
observed afternoon
FIRI-2018 F10.7 =75
FIRI-2018 F10.7=102
FIRI-2018 F10.7=130
0
25
50
75
Solar Zenith Angle (deg)

Figure 3.

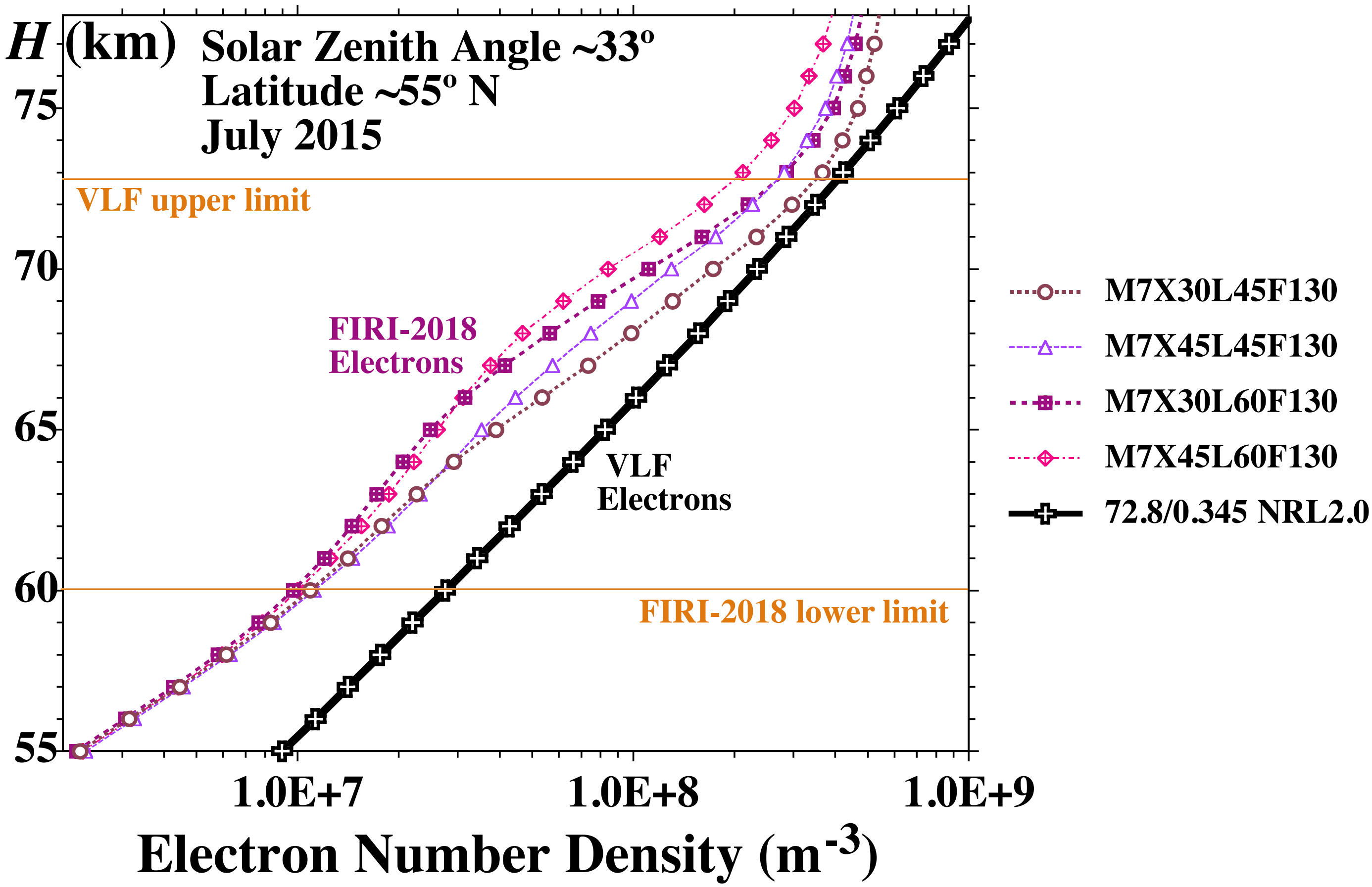

H (km)
Solar Zenith Angle ~33°
Latitude ~55° N
July 2015
VLF upper limit
FIRI-2018
Electrons
VLF
Electrons
FIRI-2018 lower limit
M7X30L45F130
M7X45L45F130
M7X30L60F130
M7X45L60F130
72.8/0.345 NRL2.0
1.0E+7
1.0E+8
1.0E+9
Electron Number Density (m-3)

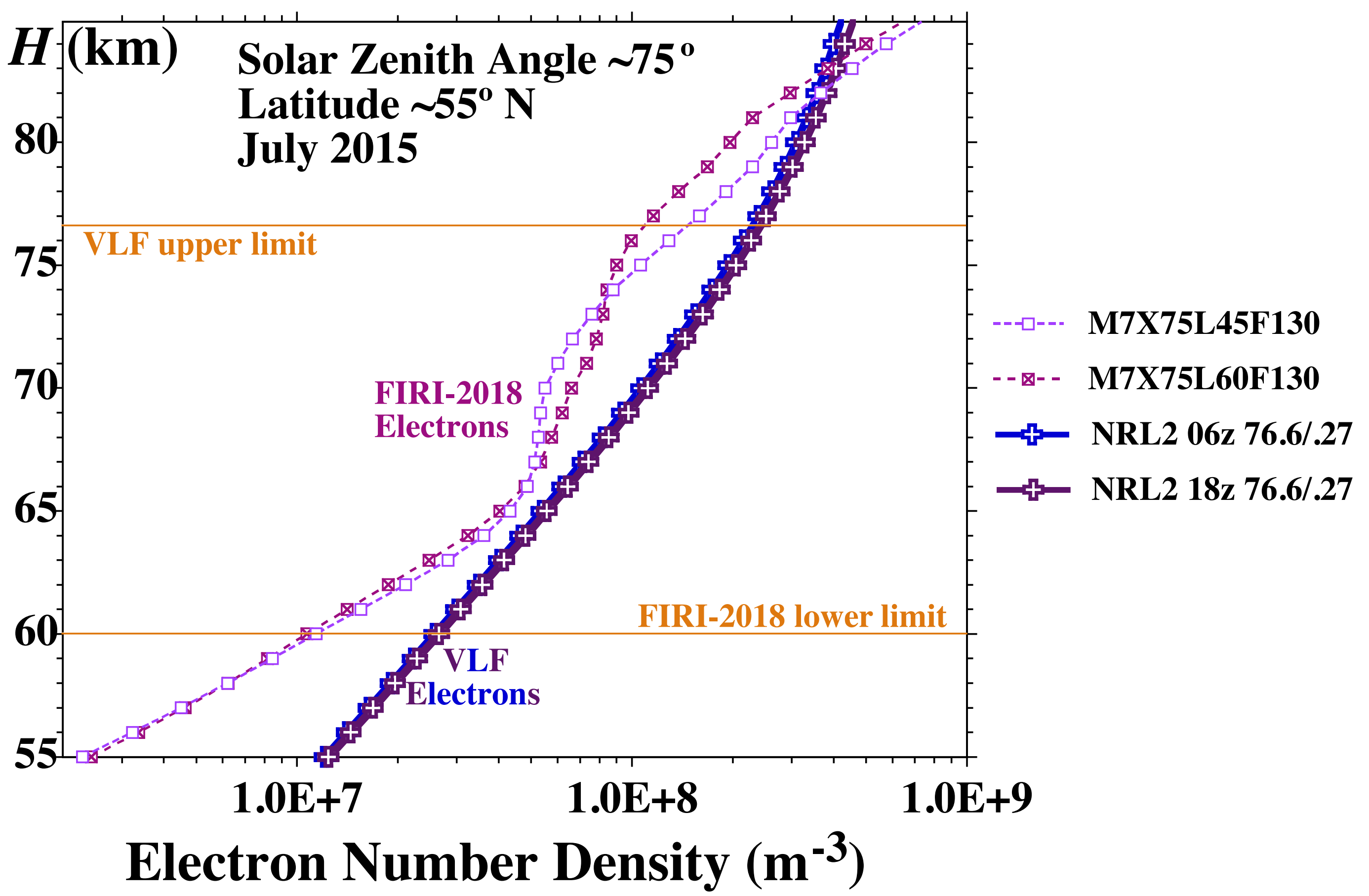

H (km)
Solar Zenith Angle ~75°
Latitude ~55° N
July 2015
VLF upper limit
FIRI-2018
Electrons
FIRI-2018 lower limit
VLF
Electrons
M7X75L45F130
M7X75L60F130
NRL2 06z 76.6/.27
NRL2 18z 76.6/.27
1.0E+7
1.0E+8
1.0E+9
Electron Number Density (m-3)

Figure 4.

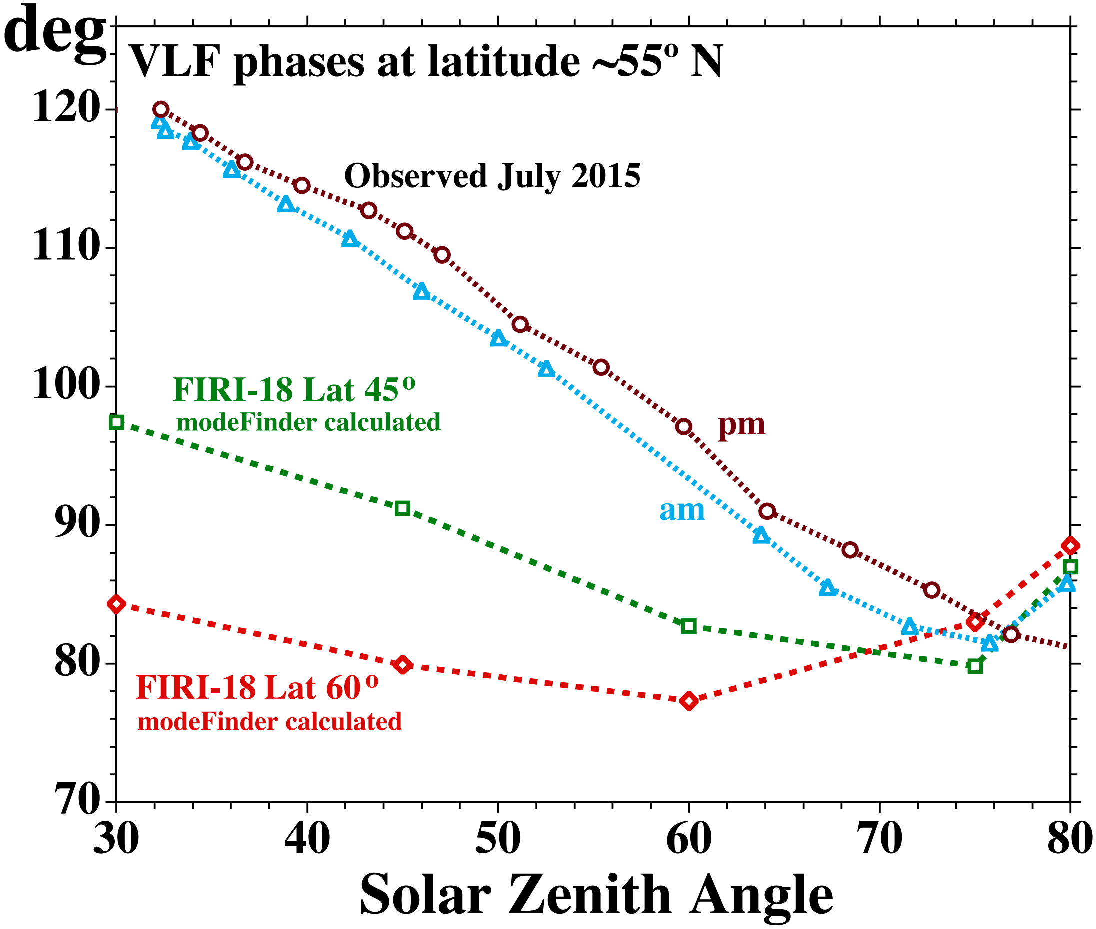
deg
VLF phases at latitude ~55° N
Observed July 2015
FIRI-18 Lat 45°
modeFinder calculated
pm
am
FIRI-18 Lat 60°
modeFinder calculated
120
110
100
90
80
70
30
40
50
60
70
80
Solar Zenith Angle

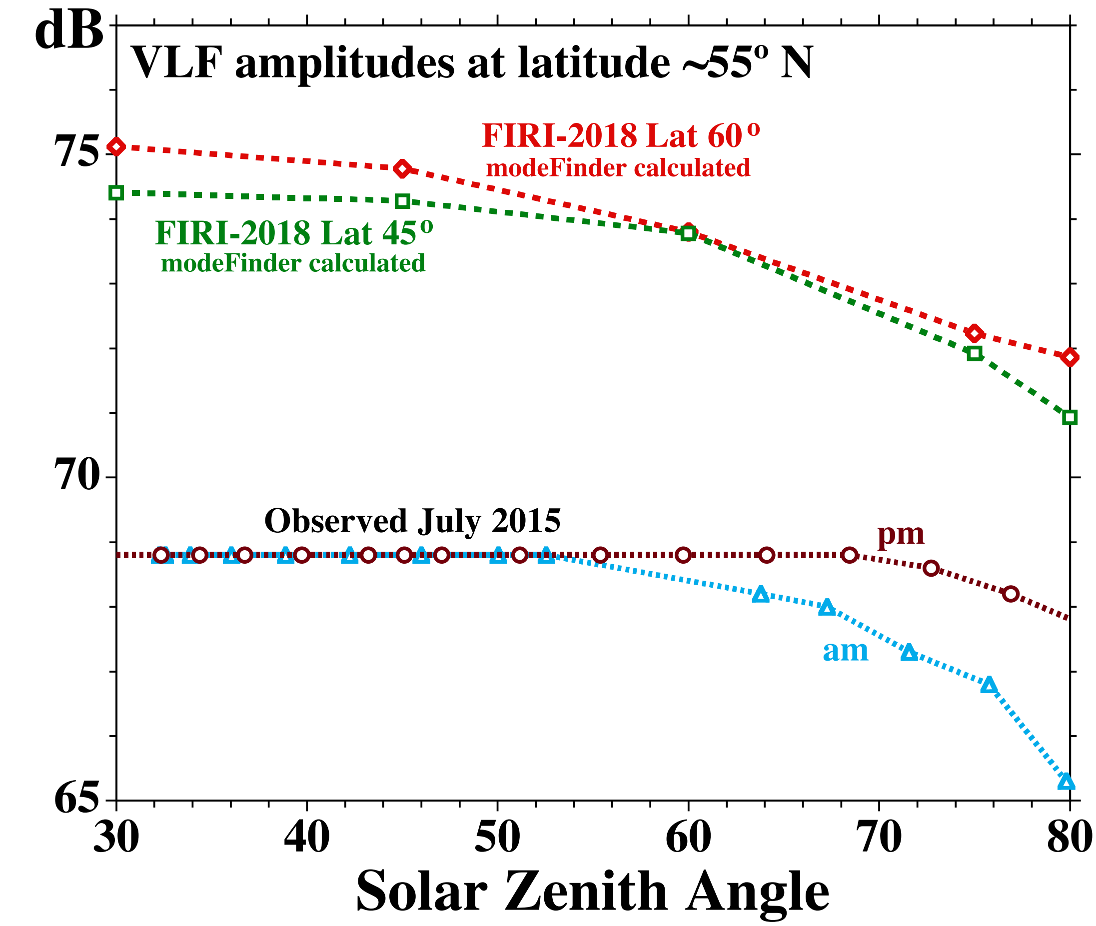
dB
VLF amplitudes at latitude ~55° N
FIRI-2018 Lat 60°
modeFinder calculated
FIRI-2018 Lat 45°
modeFinder calculated
Observed July 2015
pm
am
75
70
65
30
40
50
60
70
80
Solar Zenith Angle

Figure 5.

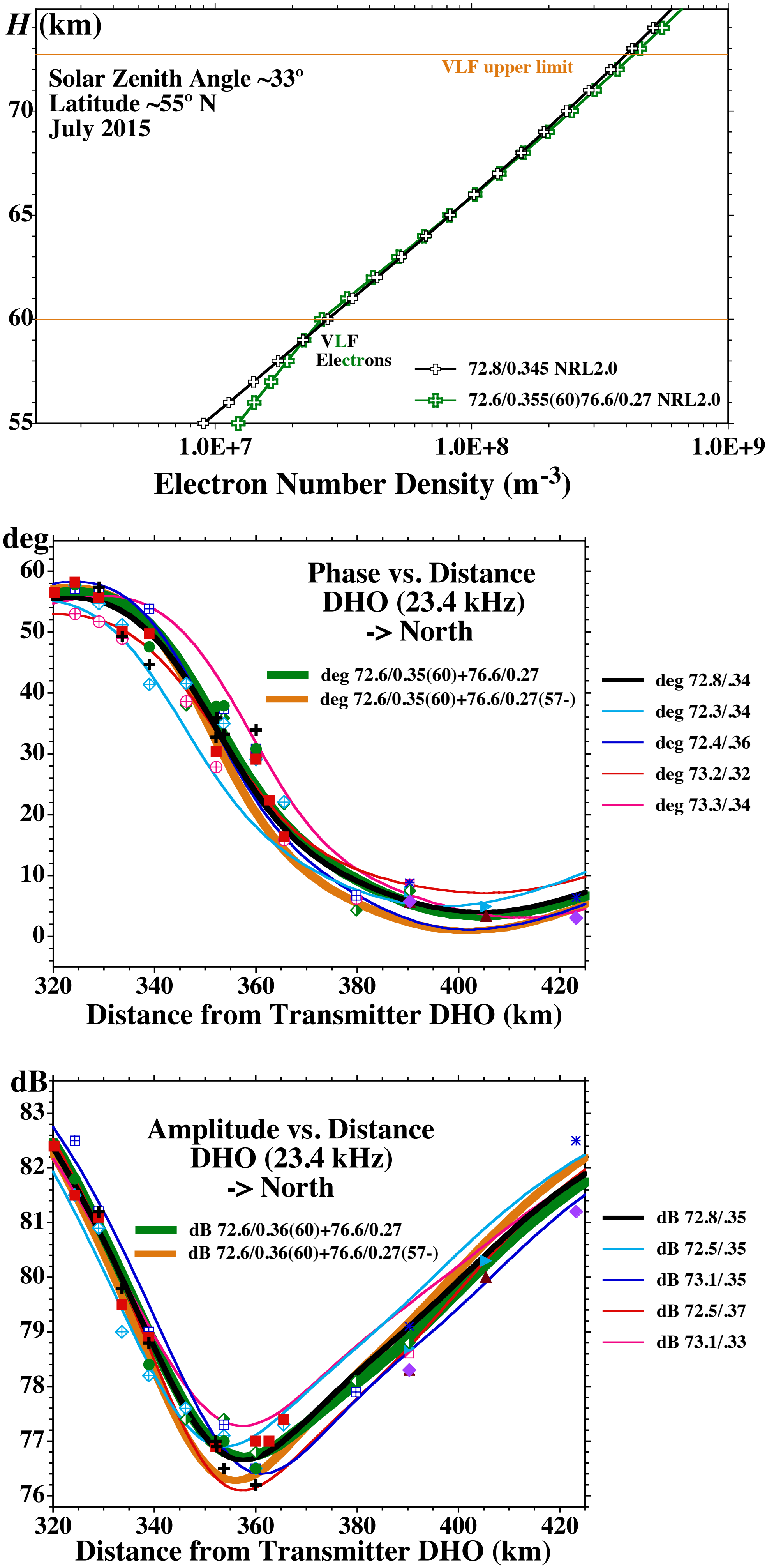

H (km)
Solar Zenith Angle ~33°
Latitude ~55° N
July 2015
VLF upper limit
VLF
Electrons
72.8/0.345 NRL2.0
72.6/0.355(60)76.6/0.27 NRL2.0
1.0E+7
1.0E+8
1.0E+9
Electron Number Density (m^-3)
deg
Phase vs. Distance
DHO (23.4 kHz)
-> North
deg 72.6/0.35(60)+76.6/0.27
deg 72.6/0.35(60)+76.6/0.27(57-)
deg 72.8/.34
deg 72.3/.34
deg 72.4/.36
deg 73.2/.32
deg 73.3/.34
Distance from Transmitter DHO (km)
dB
Amplitude vs. Distance
DHO (23.4 kHz)
-> North
dB 72.6/0.36(60)+76.6/0.27
dB 72.6/0.36(60)+76.6/0.27(57-)
dB 72.8/.35
dB 72.5/.35
dB 73.1/.35
dB 72.5/.37
dB 73.1/.33
Distance from Transmitter DHO (km)

Figure 6.

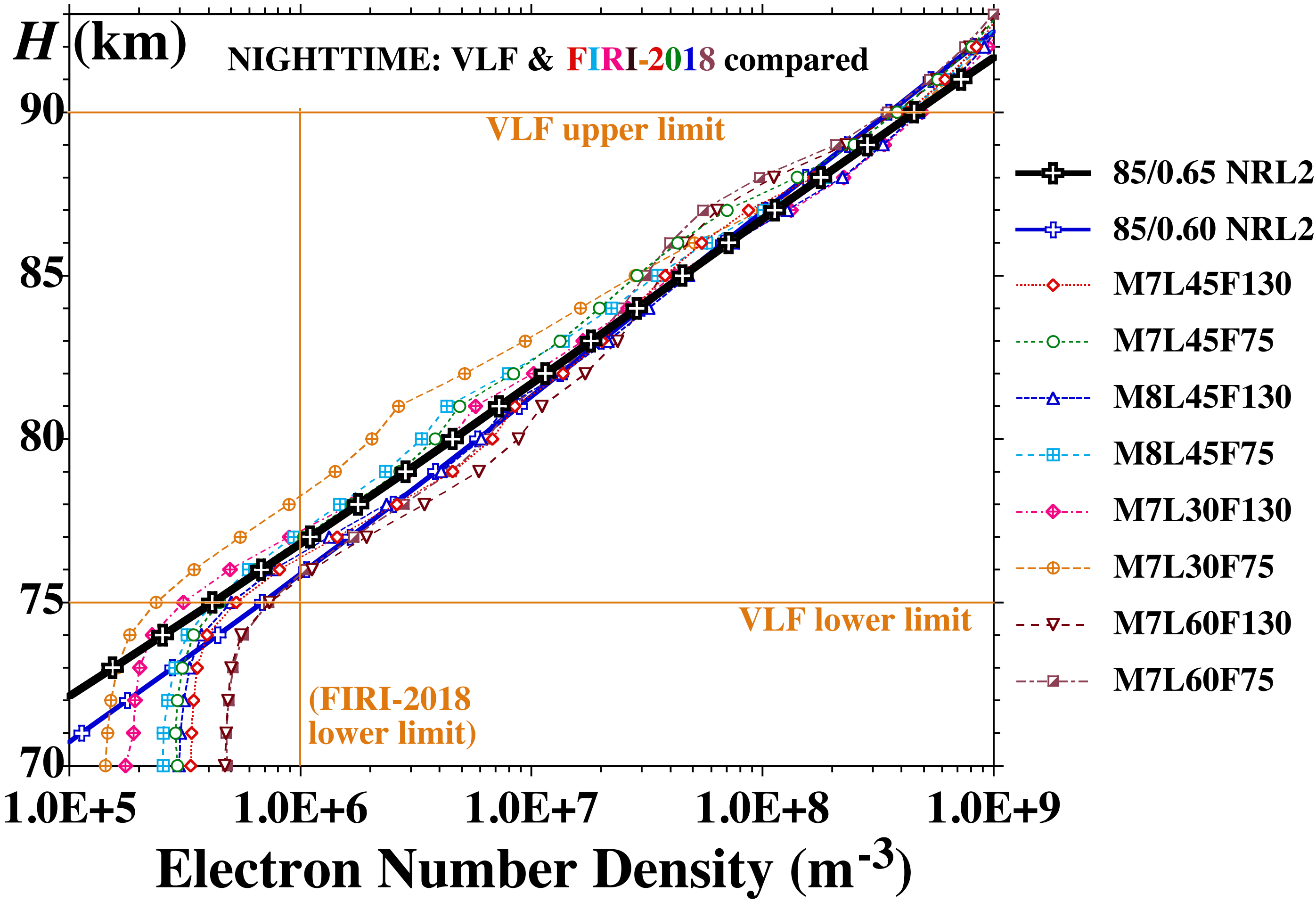

H (km)
NIGHTTIME: VLF & FIRI-2018 compared
VLF upper limit
VLF lower limit
(FIRI-2018
lower limit)
90
85
80
75
70
1.0E+5
1.0E+6
1.0E+7
1.0E+8
1.0E+9
Electron Number Density (m-3)
85/0.65 NRL2
85/0.60 NRL2
M7L45F130
M7L45F75
M8L45F130
M8L45F75
M7L30F130
M7L30F75
M7L60F130
M7L60F75

Figure 7.

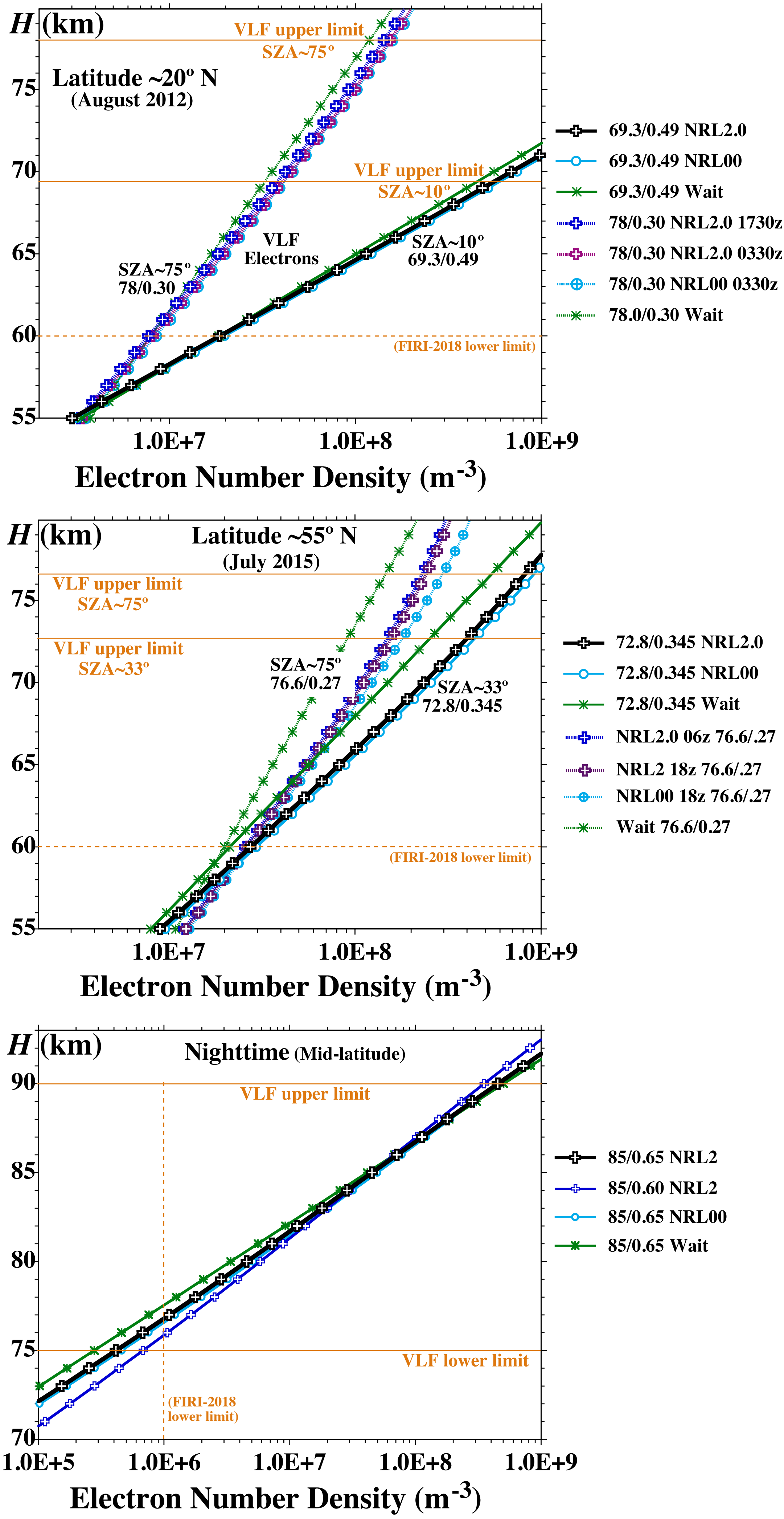

H (km)
Latitude ~20º N
(August 2012)
VLF upper limit
SZA~75º
VLF upper limit
SZA~10º
VLF
Electrons
SZA~75º
78/0.30
SZA~10º
69.3/0.49
(FIRI-2018 lower limit)
55
60
65
70
75
1.0E+7
1.0E+8
1.0E+9
Electron Number Density (m-3)
69.3/0.49 NRL2.0
69.3/0.49 NRL00
69.3/0.49 Wait
78/0.30 NRL2.0 1730z
78/0.30 NRL2.0 0330z
78/0.30 NRL00 0330z
78.0/0.30 Wait
H (km)
Latitude ~55º N
(July 2015)
VLF upper limit
SZA~75º
VLF upper limit
SZA~33º
SZA~75º
76.6/0.27
SZA~33º
72.8/0.345
(FIRI-2018 lower limit)
55
60
65
70
75
1.0E+7
1.0E+8
1.0E+9
Electron Number Density (m-3)
72.8/0.345 NRL2.0
72.8/0.345 NRL00
72.8/0.345 Wait
NRL2.0 06z 76.6/.27
NRL2 18z 76.6/.27
NRL00 18z 76.6/.27
Wait 76.6/0.27
H (km)
Nighttime (Mid-latitude)
VLF upper limit
VLF lower limit
(FIRI-2018
lower limit)
70
75
80
85
90
1.0E+5
1.0E+6
1.0E+7
1.0E+8
1.0E+9
Electron Number Density (m-3)
85/0.65 NRL2
85/0.60 NRL2
85/0.65 NRL00
85/0.65 Wait

Figure 8.

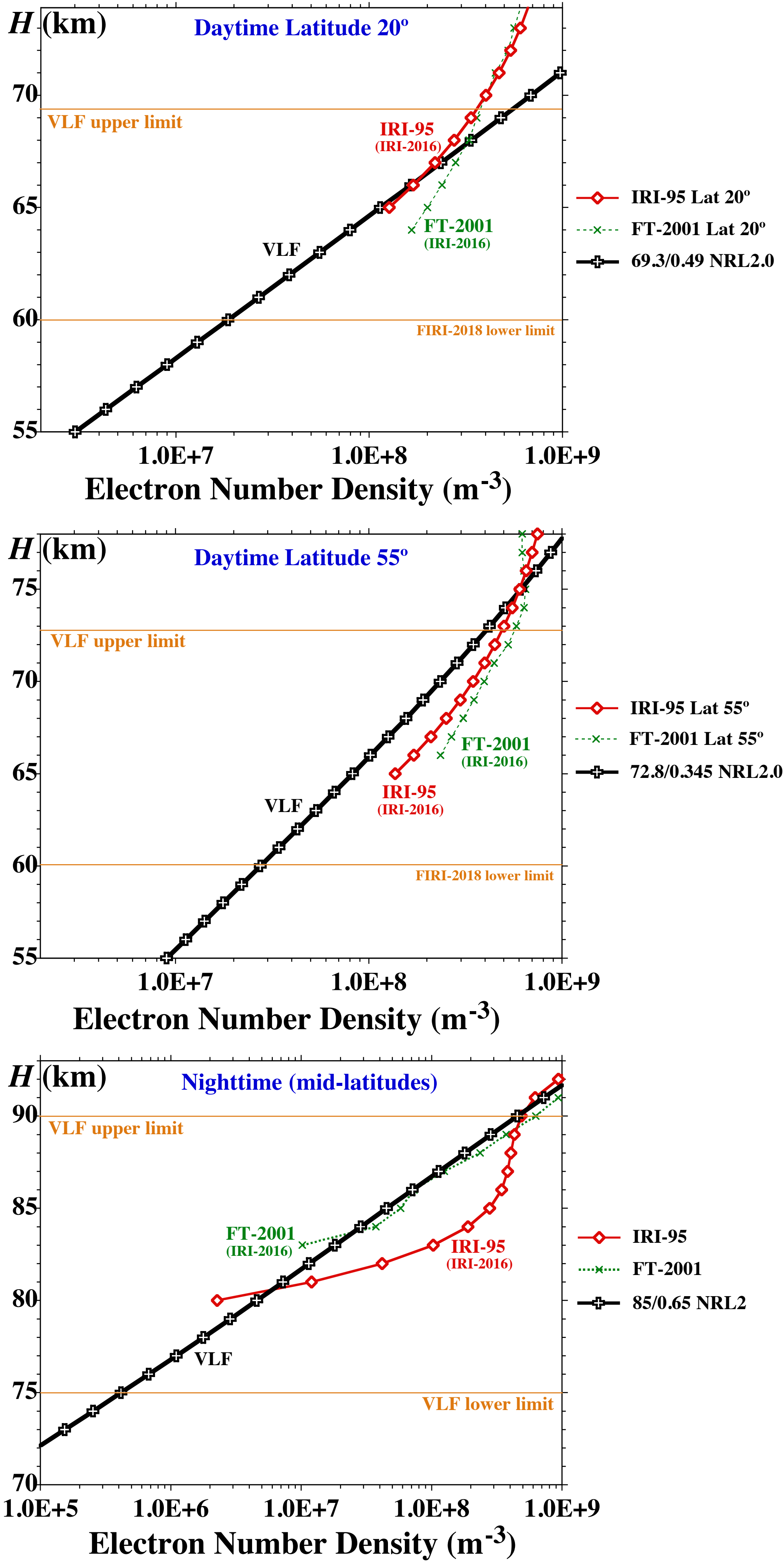
H (km)
Daytime Latitude 20º
VLF upper limit
IRI-95
(IRI-2016)
FT-2001
(IRI-2016)
VLF
FIRI-2018 lower limit
70
65
60
55
1.0E+7
1.0E+8
1.0E+9
Electron Number Density (m-3)
IRI-95 Lat 20º
FT-2001 Lat 20º
69.3/0.49 NRL2.0
H (km)
Daytime Latitude 55º
VLF upper limit
FT-2001
(IRI-2016)
IRI-95
(IRI-2016)
VLF
FIRI-2018 lower limit
75
70
65
60
55
1.0E+7
1.0E+8
1.0E+9
Electron Number Density (m-3)
IRI-95 Lat 55º
FT-2001 Lat 55º
72.8/0.345 NRL2.0
H (km)
Nighttime (mid-latitudes)
VLF upper limit
FT-2001
(IRI-2016)
IRI-95
(IRI-2016)
VLF
VLF lower limit
90
85
80
75
70
1.0E+5
1.0E+6
1.0E+7
1.0E+8
1.0E+9
Electron Number Density (m-3)
IRI-95
FT-2001
85/0.65 NRL2